JOURNAL OF GEOPHYSICAL RESEARCH, VOL. 111, C03S19, doi:10.1029/2005JC003260, 2006 [printed 112(C3), 2007]

The Adriatic Sea ecosystem seasonal cycle: Validation of a three-dimensional numerical model

L. Polimene,[1] N. Pinardi,[1] M. Zavatarelli,[1] and S. Colella[2]

Received 30 August 2005; revised 21 April 2006; accepted 14 June 2006; published 9 December 2006.

[1] A three-dimensional coupled biogeochemical-circulation numerical model was implemented in the Adriatic Sea. The biogeochemical part of the model is a development of the European Seas Regional Ecosystem Model (ERSEM II), while the circulation model is the Adriatic Sea implementation of the Princeton Ocean Model (POM). The model was run under climatological monthly varying atmospheric and river runoff forcing in order to reproduce seasonal circulation and biochemical processes. Simulated chlorophyll, nutrient, and plankton biomass and distributions were analyzed and compared with the data coming from a historic in situ data set and a newly constructed chlorophyll climatological data set from SeaWiFS. Model reproduction of the chlorophyll seasonal cycle is, at least qualitatively, in good agreement both with the remote sensing and the in situ data. However, larger production than observed is simulated during the late winter and spring, probably due to inadequate knowledge of the nutrient inputs. Comparison between simulated nutrients and observations shows a general underestimation for orthophosphate and orthosilicate, while nitrate is mostly overestimated. The shape of the nutrient-simulated profiles is in qualitatively good agreement with observations in the central and southern part of the basin. The analysis of the ratio between the large ($>20\ \mu$m) and small ($<20\ \mu$m) phytoplankton biomass and between the bacteria and phytoplankton biomass shows that the Western Adriatic Coastal Current is not only a physical frontal structure but also an ecosystem front, where larger phytoplankton grow on the coastal side while smaller ones are present offshore where the microbial loop is the dominant food web.

Citation: Polimene, L., N. Pinardi, M. Zavatarelli, and S. Colella (2006), The Adriatic Sea ecosystem seasonal cycle: Validation of a three-dimensional numerical model, *J. Geophys. Res.*, *111*, C03S19, doi:10.1029/2005JC003260 [printed *112*(C3), 2007].

1. Introduction

[2] The Adriatic Sea physical and biological oceanographic characteristics have already been extensively studied in the past. Biological Oceanography studies have dealt mainly with factors controlling dissolved nutrient concentrations and primary production processes in the Northern basin [*Franco*, 1984; *Degobbis et al.*, 1986; *Smodlaka*, 1986; *Gilmartin et al.*, 1990; *Degobbis and Gilmartin*, 1990; *Revelante and Gilmartin*, 1992]. Despite the large research effort in this area, many questions remain open about the evolution of the Adriatic Sea trophic state [*Zoppini et al.*, 1995]. Therefore Adriatic Sea trophic dynamics is still a challenge for biological oceanography.

[3] Conventionally the Adriatic Sea (Figure 1) is divided (on the basis of its morphological characteristics) in three subregions: the northern the central and the southern Adriatic Sea This partition also identifies distinct physical [*Artegiani et al.*, 1997a, 1997b] and biological [*Zavatarelli et al.*, 1998] oceanographic characteristics. From an ecological point of view the northern basin has mesotrophic to eutrophic characteristics, while the central and the southern basins show distinct oligotrophic features.

[4] In the northern part of the basin, the western coastal area has a distinct dynamical regime from the offshore zone. North of the Po delta, the near coastal area is dominated by the fresh water plumes of the many rivers, i.e., it is a ROFI area (region of fresh water influence [*Simpson*, 1997]). South of the Po delta, the circulation is dominated by a boundary intensified current, the so-called Western Adriatic Coastal Current (WACC) [*Zavatarelli et al.*, 2002] which is wind and fresh water inputs driven current. Concomitantly, the western coastal areas are dominated by the riverine discharge of land-derived nutrients [*Degobbis and Gilmartin*, 1990; *Zavatarelli et al.*, 2000]. In this area the strong, fresh water related, buoyancy input coupled with the nutrients discharge in the coastal water can give rise to higher dissolved and particulate organic carbon production and to extreme ecological phenomena such as dystrophic events and, consequently, anoxia in the bottom layers of the water column. Phenomena of strong organic matter aggregation (mucilage)

---

[1] Centro interdipartimentale per la Ricerca sulle Scienze Ambientali, Università di Bologna, Ravenna, Italy.

[2] Istituto di Scienze dell'Atmosfera e del Clima, Consiglio Nazionale delle Ricerche, Rome, Italy.

0148-0227/06/2005JC003260$09.00

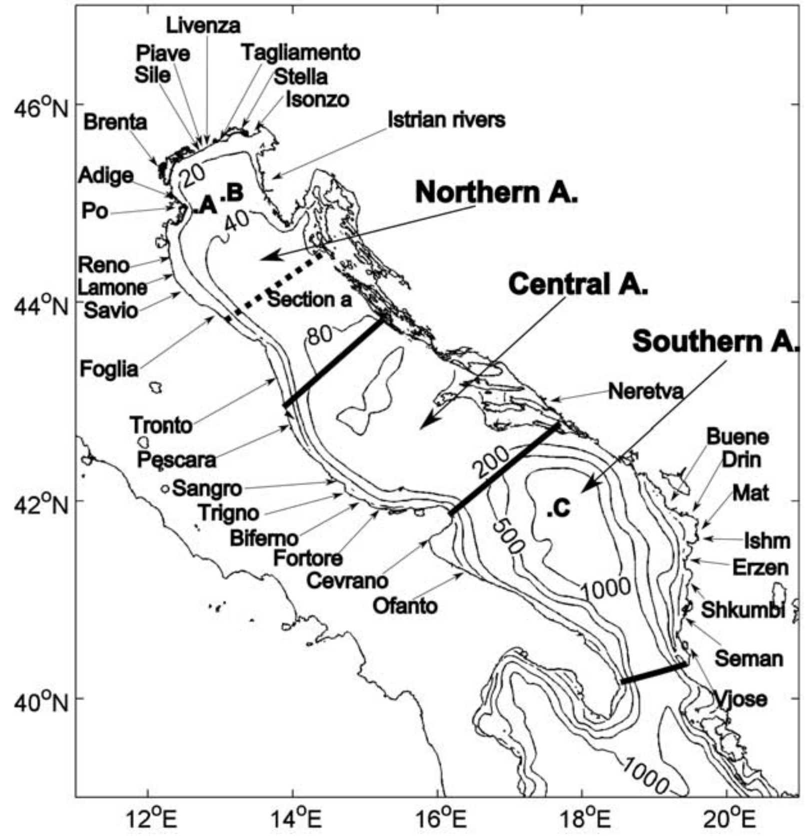

Figure 1. Adriatic Sea morphology, subbasin partitions, and river mouth locations. Section a and points A, B, and C are mentioned into the text and Figures 13 and 15.

are also periodically observed in offshore areas of the northern Adriatic [*Giani et al.*, 2005] but their nature and formation is outside the scope of the present paper since the events do not present a seasonally recurrent phenomena but rather an interannual signal.

[5] The central and southern regions of the Adriatic Sea are characterized by lower primary production, with the continental input and the benthic pelagic interactions being of minor importance in comparison to the northern area [*Zavatarelli et al.*, 2000]. Exceptions are the southeastern coastal areas where Albanian river discharges are certainly an important (albeit almost unquantified) nutrient source. The western coastal areas of both the central and southern Adriatic are affected by the extension of the WACC which carries chlorophyll reach waters from the northern basin areas. The offshore central and southern Adriatic, however, show clearly oligotrophic characteristics [*Vilicic et al.*, 1989] and the primary production cycle is regulated by the nutrient supply to the euphotic zone from the deep part of the water column by different upwelling and mixing processes [*Zavatarelli et al.*, 2000]. The circulation is characterized by different cyclonic gyres which in turn show enhanced upwelling at their centers. The deep supply of nutrients is related to the Modified Levantine Intermediate Water (MLIW) entering the Adriatic from the Ionian Sea through the Otranto Channel [*Zavatarelli et al.*, 1998].

[6] Given such complex dynamics, it is necessary to develop a numerical model that can produce future scenarios of the ecosystem trends and this paper is concerned with the construction and validation of such a model. In fact, we show the first simulations of the seasonal primary production cycle from a high-resolution three-dimensional coupled physical-biogeochemical model of the marine trophic food web, implemented for the first time in the Adriatic Sea with realistic basin lateral (river inputs) and atmospheric forcing. The first implementation was in an highly idealized basin-scale model [*Zavatarelli et al.*, 2000] where it was not really possible to study the coupling between basin circulation features and biogeochemistry. The basin was in fact idealized and composed of a rectangle with a sloping bottom mimicking the basin bathymetry. The model here presented has, instead, a realistic geometry and in particular realistic river runoff and nutrient loadings. The coexistence of coastal-eutrophic and open ocean oligotrophic conditions implies a north to south and west to east trophic gradient, which is one of the most important ecological characteristics of the Adriatic sea and we will show that an ecosystem model can quite faithfully reproduce this.

[7] The model is validated with the available observations both in situ and from satellite: in order to do this a new climatology from SeaWiFS has been produced for the intercomparison. One of the major results of the paper is the description of the distribution of biochemical state variables and their correlation with physical structures. This is the first part of a work that in the future will develop sensitivity experiments to the ecosystem parameters giving rise to a more complete understanding of the biochemical processes occurring in the Adriatic Sea ecosystem.

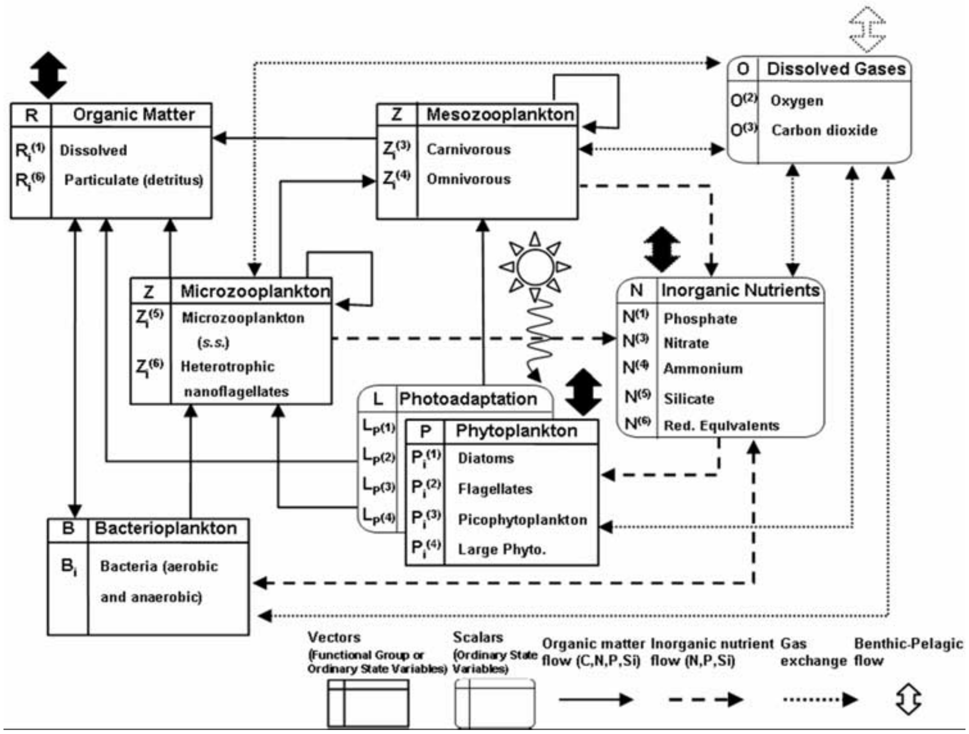

Figure 2. General overview of the biogeochemical state variables and matter fluxes implemented in the ERSEM pelagic module. Square boxes represent functional groups defined in the model. Solid arrows indicate fluxes of carbon and inorganic nutrients, dashed arrows indicate fluxes of inorganic nutrients, and dotted arrows indicate the gas exchange. From *Vichi et al.* [2003], reprinted with permission from Copernicus Publications.

[8] In the next section we describe the model equations and assumptions, in section 3 the model implementation in the Adriatic Sea and in section 4 the results are described and discussed. A general conclusion is offered in section 5.

2. Numerical Model

[9] The three-dimensional ecosystem numerical model used in the present study is the coupling of a biogeochemical with a hydrodynamic model. The biogeochemical pelagic model is a development of the European Sea Ecosystem Model (ERSEM) [*Baretta et al.*, 1995; *Vichi et al.*, 1998, 2003], which is fully described by *Blackford et al.* [2004] to which we added a new bacteria-DOM submodel described by *Polimene et al.* [2006]. The circulation model is the Adriatic Sea implementation [*Zavatarelli and Pinardi*, 2003] of the Princeton Ocean Model (POM) with perpetual year forcing.

2.1. Biogeochemical Flux Model

[10] A schematic description of the biochemical flux model used for the pelagic components is given in Figure 2. This model is based upon the *Baretta et al.* [1995] ERSEM code and has been called Biochemical Flux Model, hereafter BFM.

[11] BFM is a modeling framework representing the marine ecosystem as a set of interacting physical, chemical and biological processes. The "functional group" approach is used to describe the biota, which is subdivided into three main functional types: primary producers, consumers and decomposers. These broad groups are then subdivided on the basis of trophic links and/or size. It should be noted that individual species may straddle more that one functional group, and that the functional groups describe particular types of behavior rather than species lists. Each functional group is defined by a number of internal constituents, namely carbon, nitrogen, and phosphorus and, in the case of diatoms, silicon, each of which is explicitly modeled. Physiological (ingestion, respiration, excretion and egestion) and population (growth and mortality) processes are included in the descriptions of functional group dynamics. These dynamics are described by fluxes of internal constituents among functional groups.

[12] The model is generic and has been demonstrated to simulate a wide range of ecosystems from temperate eutrophic coastal waters, to upwelling areas and the ultra oligotrophic eastern Mediterranean without making significant changes in the parameterization [*Blackford et al.*, 2004]. A summary of the equations, for primary producers functional groups representation, is given in Appendix A.

[13] A simple benthic return model has been used instead of the more complex benthic model used by *Zavatarelli et al.* [2000] since tuning of the benthic parameters is difficult due to the scarcity of data for initial conditions. In order to parameterize the benthic remineralization, a fixed quota (1% per day) of each detritus component (C, N, P, Si) reaching the bottom is reinjected to the water column as dissolved nutrients and carbon dioxide.

2.2. Coupling Between POM and the BFM

[14] The coupling between the two models is schematically represented in Figure 3. At each model time steps (900 s) the hydrodynamics provides the BFM with information about the physical environment which is then held

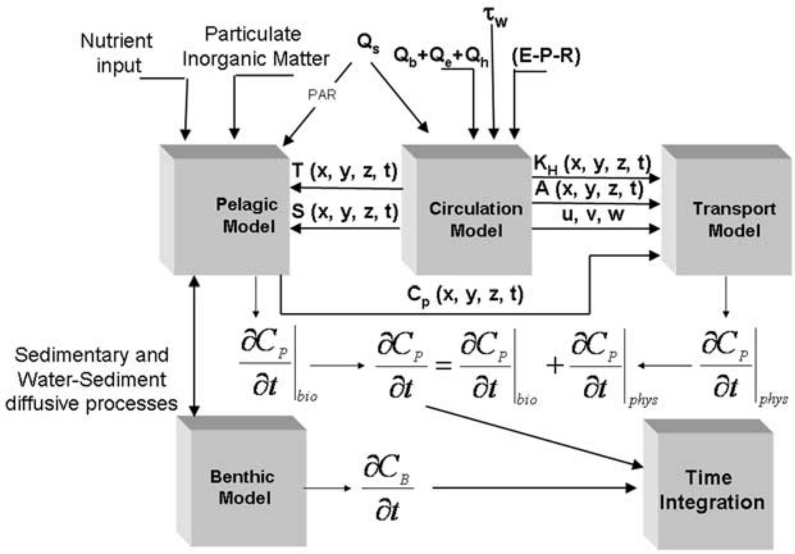

Figure 3. POM ERSEM coupling scheme. Here $\frac{\partial C_p}{\partial t}$ is the total rate of change of a generic biochemical variable C_p, $\left.\frac{\partial C_p}{\partial t}\right|_{phys}$ is the rate of chance due to physical processes, and $\left.\frac{\partial C_p}{\partial t}\right|_{bio}$ is the rate of change due to the biogeochemical processes. Q_s is the solar radiation flux; Q_h, Q_e, and Q_b are the sensible, latent, and longwave radiation fluxes emitted at the surface (in W m^{-2}). K_H is the vertical diffusion coefficient for scalar properties, and A is the horizontal diffusion coefficient; τ_w is the wind stress. E-P-R is the saltwater/freshwater flux (evaporation-precipitation-runoff).

constant for the biochemistry. BFM receives information about temperature to calculate the metabolic response of biota and salinity to calculate oxygen saturation. The advective and diffusive rate of change of each pelagic state variable is determined from the velocity fields, horizontal and viscosity coefficients generated by POM and this is called the physical rate of change of the biochemical state variable C:

$$\left.\frac{\partial C}{\partial t}\right|_{phys} = -u\frac{\partial C}{\partial x} - v\frac{\partial C}{\partial y} - w\frac{\partial C}{\partial z} + F_C \tag{1}$$

where u, v, w are the velocity components and F_C is the divergence of the turbulent eddy fluxes, mixing and dispersing the tracers with turbulent stresses. Since the numerical advective scheme used in (1) is simply a centered finite difference scheme, negative values in C can appear. However, a check is carried out at each time step on these negative values and the negative values are changed to zero. This amounts to having a tracer increase of only a few% for the 4-year-long integration showed in this paper without trends. We decided to leave the advective scheme of POM unaltered because other schemes were too diffusive at the model resolution used and the tracer unbalance was not relevant.

[15] The rate of change due to biochemical processes is $\left.\frac{\partial C}{\partial t}\right|_{bio}$. The processes contained in this term, for the phytoplankton functional groups, are described in Appendix A. The total rate of change is then defined by

$$\left.\frac{\partial C}{\partial t}\right|_{tot} = \left.\frac{\partial C}{\partial t}\right|_{phys} + \left.\frac{\partial C}{\partial t}\right|_{bio} \tag{2}$$

that is the coupled equation of the ecosystem model used for all the state variables of the BFM. In addition to physical transport, for some of the BFM state variables, a sinking velocity was added to the vertical advective term in (1) to parameterize large falling velocities of material. Equation (2) is solved with an Euler forward time integration scheme described by *Zavatarelli et al.* [2000]. The coupled equation (2) can be unstable since the $\left.\frac{\partial C}{\partial t}\right|_{bio}$ can be very large when there is phytoplankton bloom. Thus the coupler realizes a “time step cutting” procedure up to the point where the equation is once again numerically stable. The physical fields during time step cutting are held constant.

[16] Another important coupling between physics and BFM is given by visible light incident at the surface. The physical model uses a realistic parameterization of surface solar radiation, Q_s, for the Adriatic Sea [*Maggiore et al.*, 1998] but this value has to be transformed into PAR (photosynthetically available radiation). We assume a multiplicative constant factor of 0.5 in front of Q_s to have the amount of light available for photosynthesis. In this model we do not assume any feedback between biology and physics yet but the BFM considers adaptation to light by the phytoplankton as described by *Ebenhöh et al.* [1997].

3. Model Implementation in the Adriatic Sea

3.1. Grid and Bathymetry

[17] The model domain (Figure 1) encompasses the whole Adriatic basin and extends south of the Otranto channel into the northern Ionian Sea, where the only open boundary is located.

[18] The model grid has an horizontal resolution of approximately 5 km. In the vertical the model uses 21 σ levels, where $\sigma = (z - \eta)/(H + \eta)$; H (x, y) is the bottom topography and η(x, y, t) is the free surface elevation. The

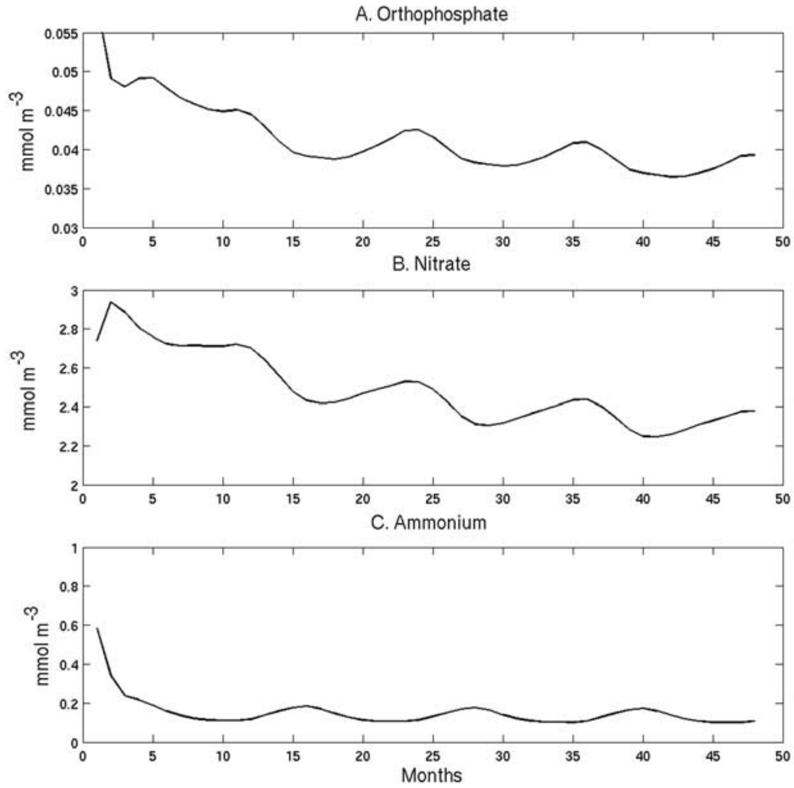

Figure 4. Adriatic Sea nutrient basin means in the 4 year coupled model run. (a) Orthophosphate, (b) nitrate, and (c) ammonium.

sigma layers have a logarithmic distribution near the surface and the bottom.

[19] The model bathymetry was obtained from the U.S. Navy 1/60° bathymetric database DBDB1, by bilinear interpolation of the depth data into the model grid.

[20] The minimum depth of the model is 10 m so that coastal processes are resolved up to this depth. This choice is dictated by the model domain extension which contains deep bathymetry such as in the Ionian and the need to resolve vertical processes there. Shallower coastal processes can be resolved in the future with a nested approach.

3.2. Physical Initial and Boundary Conditions

[21] The physical model implementation is exactly the same as that of *Zavatarelli and Pinardi* [2003] and will not repeated in detail here. The physical model has been spun up for three years with climatological atmospheric forcing so that a repeating seasonal cycle was obtained in the basin mean temperature and salinity volume mean values.

[22] The coupled model is started from the third year winter distributions of the physical fields. After that the coupled model is run for an additional four years with physical conditions that repeat identically every year while the biochemistry is spun up from idealized initial conditions described below. Thus in conclusion we spin up first the physical model and then, with realistic circulation features, we let the BFM evolve up to a repeating seasonal cycle.

3.3. Initial Conditions for the Biogeochemical Model

[23] The initial conditions for the nutrients have been estimated from the ABCD data set [*Zavatarelli et al.*, 1998] climatological winter averages and are assumed to be horizontally homogeneous but vertically variable. Initial condition for phytoplankton, zooplankton and bacteria biomass have been taken from the initial conditions for the ERSEM North Sea model, assuming low biomass in winter. The initial condition for pelagic biomass were reduced by 2 orders of magnitude below the euphotic zone.

[24] The distribution of sediments is prescribed since no benthic resuspension/deposition processes are considered and no loads of sediments from the rivers. The initial condition is given by the profile described by *Vichi et al.* [1998].

3.4. Lateral and Vertical Biogeochemical Boundary Conditions

[25] For the BFM no atmospheric input of nutrients was considered. The lateral boundary conditions for nutrient loads were parameterized as for the case of salinity, i.e., as a vertical flux of nutrients at the river mouth points. Only dissolved nutrients were considered while no particulate, dissolved organic and sediment inputs were considered.

[26] Nutrient river inputs (N (= PO_4, NO_3, SiO_2, NH_4)) were introduced into the model by using the river nutrient annual mean load, N_0, multiplied by the monthly varying runoff (R) to obtain a surface nutrient flux boundary condition in the following way

$$K_\nu \frac{\partial N}{\partial z}\bigg|_{z=0} = \frac{R(t)N_o}{\int_1^{12} R(t)dt}(\Delta x \Delta y)^{-1} \tag{3}$$

where K_ν is the vertical eddy diffusivity. The integral is done on the twelve monthly mean runoff values and R is given only at the mouth grid points. The fresh water sources are taken from *Zavatarelli and Pinardi* [2003]. In Figure 1 the freshwater input points (corresponding to the major Adriatic rivers mouth locations) are indicated along with considered nutrient input points.

[27] The Po river runoff was distributed along more grid points, in order to represent the freshwater discharge and nutrient loads of the various mouths of the delta. Mouth partitioning of the Po total runoff was defined according to the estimates reported by *Provini et al.* [1992].

[28] The mean river nutrient loads were taken from the *Degobbis and Gilmartin* [1990] estimates for the Po river. This corresponds to a nitrate, orthophosphate, ammonium and orthosilicate load of 7347, 230, 1056 and 5990 106 mol/yr respectively. These values were used in (3) and distributed in the different Delta mouths following the proportions of *Provini et al.* [1992]. For the other rivers the annual mean load, for each nutrient, was supposed to be a fraction of that one of the Po river, respectively 20% for the Albanian rivers (from Vjose to Neretva, see Figure 1) 10% for the Istrian rivers and 50% for all the others.

[29] Concerning the lateral open boundary in the Ionian Sea we used the same open boundary condition scheme implemented for temperature and salinity. For a BFM state variable, C, we find the value of the concentration at outflow, $C_{O.B}$, using an upwind equation written as

$$\frac{\partial C_{O.B.}}{\partial t} + V_{O.B}\frac{\partial C_{O.B}}{\partial y} = 0 \qquad (4)$$

where $V_{O.B}$ is the meridional velocity normal to the zonal open boundary prescribed from the physical model. At inflow, C is prescribed to be equal to an assigned value, C_{fix},

$$C_{O.B} = C_{fix}. \qquad (5)$$

where C_{fix} is a vertical profile estimated for each biogeochemical variables from the ABCD data set.

4. Results and Discussion

[30] In this section we discuss the simulation results and we intercompare them with climatological observations from the ABCD data set [*Zavatarelli et al.*, 1998] and, for chlorophyll, with remote sensing data. The climatological, monthly averaged, chlorophyll *a* data arise from seven years (1998–2004) of SeaWiFS ocean color observations with 1 Km spatial resolution generated using the OC4v4 algorithm [*O'Reilly et al.*, 2000] implemented on SeaDAS software. Data were flagged for clouds or other contamination factors (land, Sun glint, atmospheric correction failure, high total radiance, large solar zenith angle, large spacecraft zenith angle, coccolithophores). For the comparison with simulations, remote sensing data have been linearly interpolated on the model grid.

[31] As described in the introduction, the Adriatic Sea has been divided into three different regions (see Figure 1), the northern, central and southern subbasin. For the comparison with the ABCD data the northern basin is further subdivided into a shallower region (the truly coastal area) and a deeper region, separated by the 40-m isobath. Both observed and simulated nutrients profiles were averaged in the four subbasin and, then, compared.

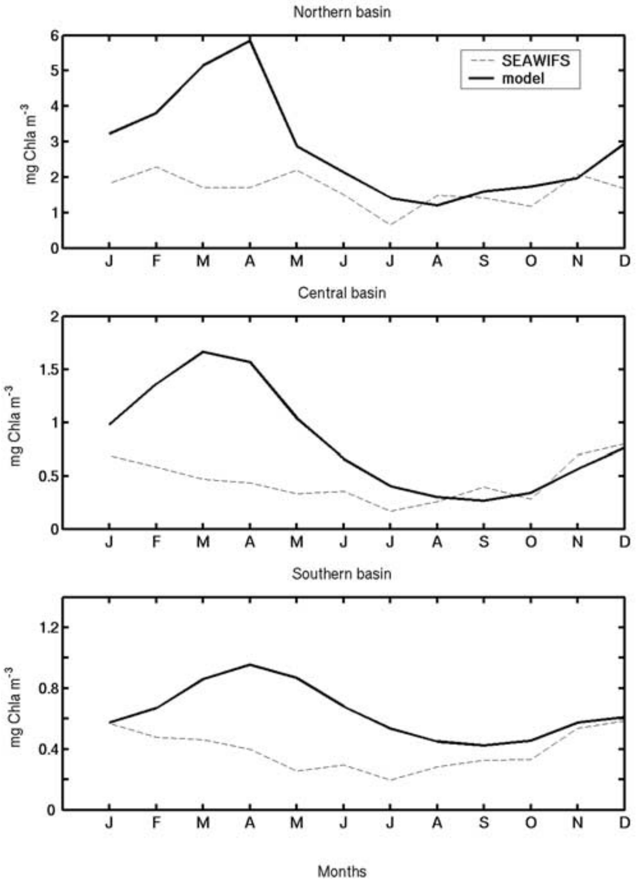

Figure 5. Chlorophyll *a* (mg Chl a/m^3) annual cycle estimated from SeaWiFS data and model simulations. Values are averaged in the northern, central, and southern Adriatic basin. Simulated chlorophyll concentrations are averaged on the *e*-folding depth of the PAR.

[32] Because of the not homogeneous spatial distribution of the chlorophyll observations, model derived chlorophyll profiles were computed by considering only parts of the model domain that are matched by an homogeneous ABCD data spatial coverage.

[33] Seasons are defined as follows: winter is from January to March, spring from April to June, summer from July to September and autumn from October to December.

4.1. Biogeochemical Spin-up Problem

[34] Results shown in the following sections are extracted from the fourth year of the coupled model run. To check whether the biogeochemical state variables reached a stable repetitive cycle, a check on the volume averaged time series of selected state variables (orthoposphate, nitrate and ammonium) was computed. Orthophosphate (Figure 4a), nitrate (Figure 4b), and ammonium (Figure 4c) reach an almost stable seasonal cycle after three years of simulation. As expected, maximum concentrations are reached in winter and in autumn in correspondence of the maximum climatological river runoff [*Raicich*, 1994, 1996].

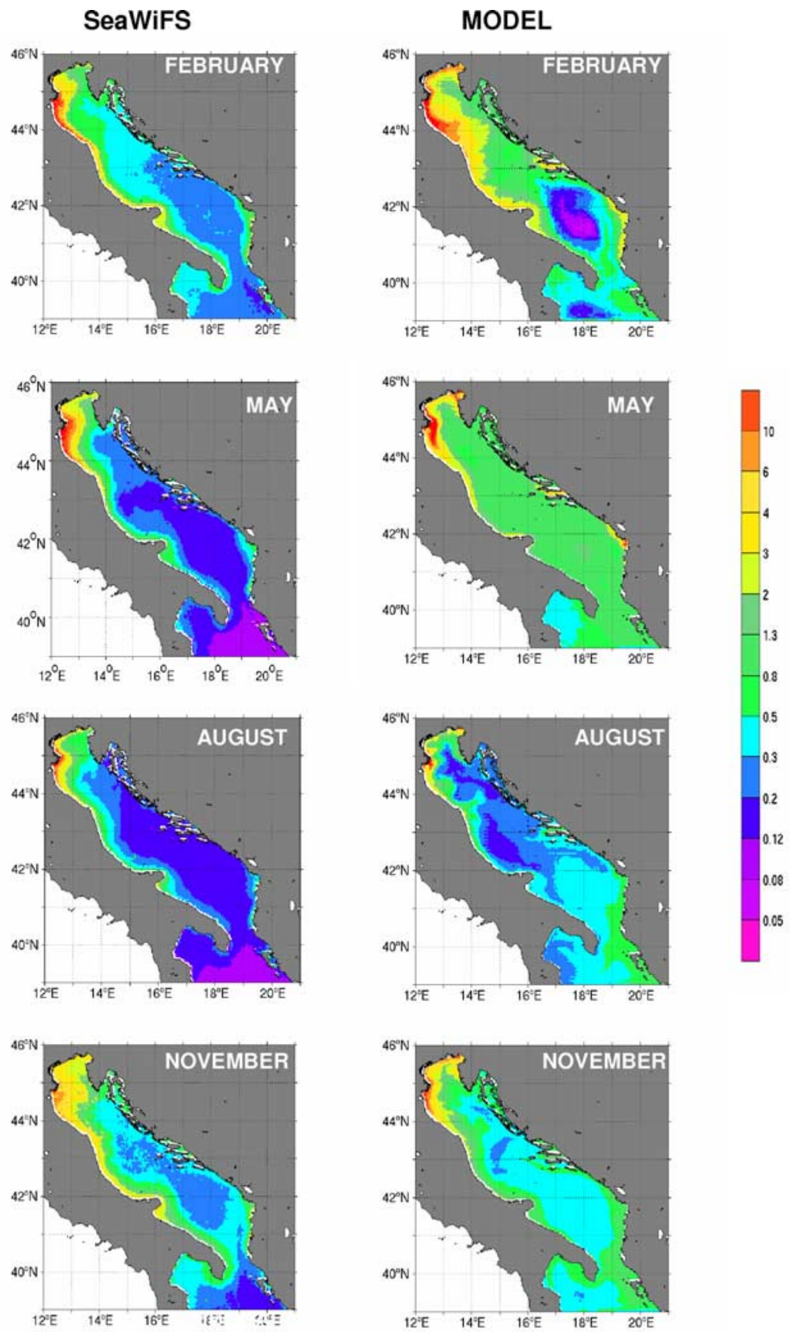

Figure 6. Chlorophyll *a* monthly mean concentration (mg Chl a/m^3) from SeaWiFS data and from model simulations. Simulated chlorophyll concentrations are averaged on the *e*-folding depth of the PAR.

4.2. Chlorophyll *a*

[35] Modeled chlorophyll *a* has been estimated by dividing the biomass of the four phytoplanktonic functional groups present in the BFM for a fixed conversion factor which is 50 for flagellates, picophytoplankton and dinoflagellates and 25 for diatoms [*Baretta et al.*, 1995]. In order to compare simulations with remote sensing data, modeled chlorophyll has been averaged on the *e*-folding depth of the PAR.

[36] The temporal trend of the monthly averaged chlorophyll a concentration both simulated and estimated from remote sensing data for the northern, central, and southern Adriatic basins is shown in Figure 5, while in Figure 6 the monthly averaged (for selected months) chlorophyll distributions are shown for the whole Adriatic basin.

[37] Temporal evolution of the simulated chlorophyll *a* have a larger seasonal cycle than that depicted by the remote sensing data. Simulated values overestimate the SeaWiFS data in winter and spring, while are in good agreement with them in summer and autumn.

[38] The observed decrease of chlorophyll *a* concentration from the northern to the southern subbasin is, at least qualitatively, well reproduced by the model. The north-south gradient is also evident from the analysis of the

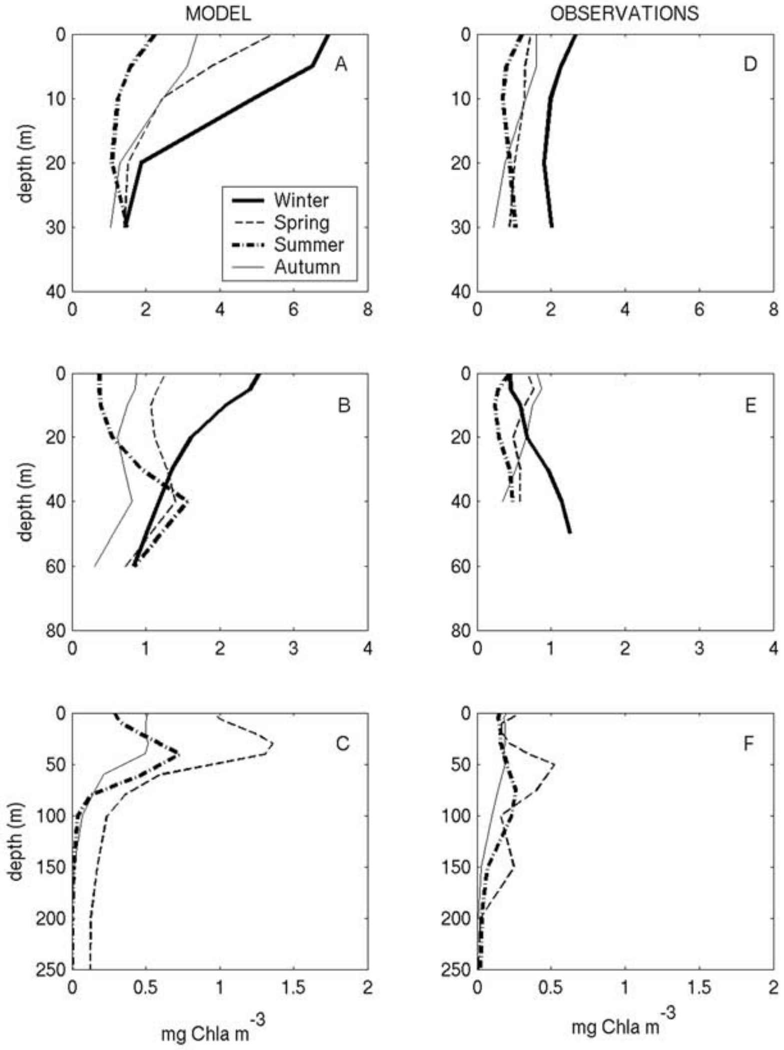

Figure 7. Seasonally mean chlorophyll *a* (mg Chl *a*/m^3) subbasin averaged profiles for (a, b, c) model and (d, e, f) observations. Figures 7a and 7d are shallow north; Figures 7b and 7f are deep north; Figures 7c and 7g are central basin.

modeled chlorophyll *a* distribution (Figure 6) that also highlights the capacity of the model to reproduce the west-east Adriatic Sea trophic gradient in a way that is consistent with the remote sensing data.

[39] The model reproduces, in all months considered, the high concentration values present in the northern basin and along the western coast. The steep decrease of chlorophyll *a* moving toward the offshore areas is also well captured by the simulations. The distribution of the high chlorophyll *a* values along the western coast is clearly governed by the nutrient input from the Po river and by the circulation causing southward advection of the phytoplankton [*Zavatarelli et al.*, 2002]. The Po river nutrient discharge causes a permanent bloom condition, in the area proximal to the Po delta, with chlorophyll *a* concentration values higher than 10 mg/m^3, a value consistent with the remote sensing values.

[40] The chlorophyll *a* overestimation in late winter-spring is particularly evident in the offshore area of the central and southern basins where the simulations are able to reproduce only qualitatively the SeaWiFS data: simulated chlorophyll *a* concentrations range from 0.5 to 2 mg/m^3, while, the SeaWiFS data range from 0.3 to 0.5 mg/m^3.

[41] In August and November the agreement between model and remote sensing is generally good in terms of both values and distribution. In August the main discrepancy is present in the southern basin where the simulated chlorophyll a is slightly higher with respect to the satellite data, while, in November, in the central part of the northern basin, simulations are slightly lower with respect to the SeaWiFS data.

[42] It can be argued that the winter overestimation may be due to a inaccurate definition of the river nutrient discharge. In fact, the river nutrient input was defined by estimating the mean river water concentration, without considering removal and transformation processes possibly occurring through the river mouth, which may cause a significant reduction of the nutrient loading. An overestimation of the nutrient upwelling processes related to the cyclonic circulation in the southern Adriatic could also be involved in determining the discrepancy between remotely sensed observations and simulations.

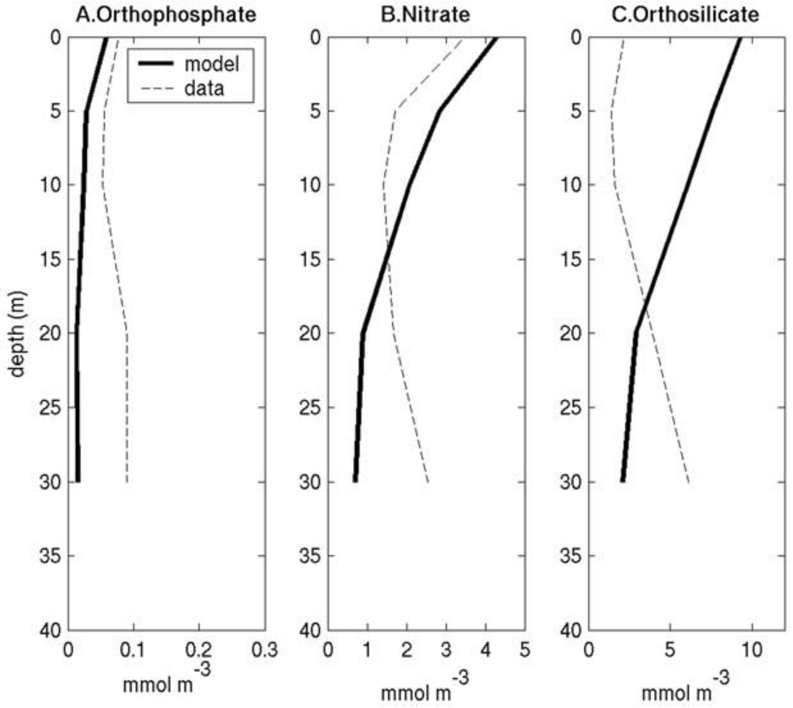

Figure 8. Mean simulated and observed nutrients annual profiles averaged in the shallow northern basin. (a) Orthophosphate (mmol/m^3); (b) nitrate (mmol/m^3); (c) orthosilicate (mmol/m^3).

[43] A comparison of the seasonally mean chlorophyll *a* vertical profiles averaged in the subbasins defined in Figure 1 with the corresponding profiles from the ABCD data set is shown in Figure 7.

[44] In the northern shallow basin the simulated chlorophyll *a* reaches the maximum value (about 7 mg m^{-3}) in winter in the first 5 m of the water column, while, is constantly above this value throughout the year. Below

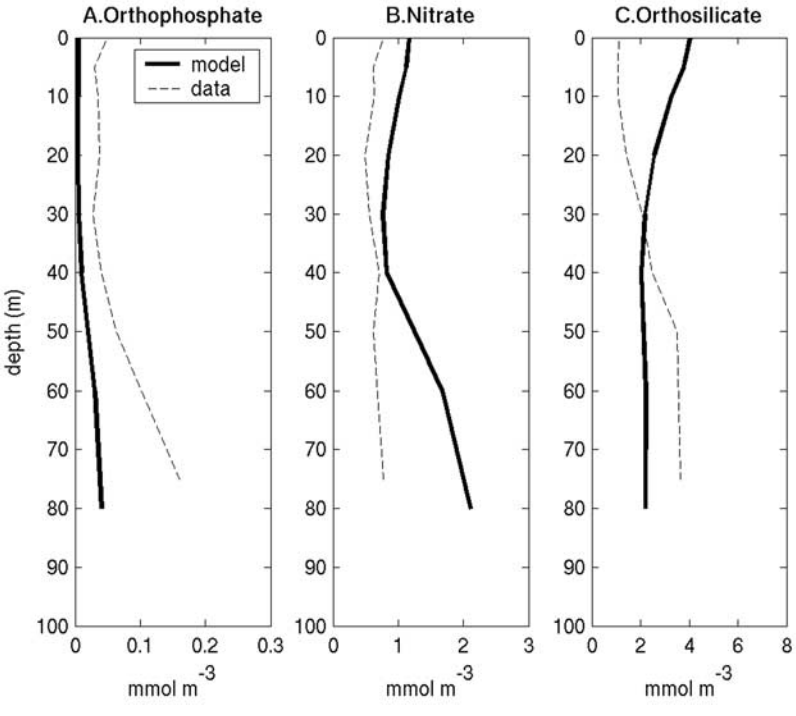

Figure 9. Mean simulated and observed nutrients annual profiles averaged in the deep northern basin. (a) Orthophosphate (mmol/m^3); (b) nitrate (mmol/m^3); (c) orthosilicate (mmol/m^3).

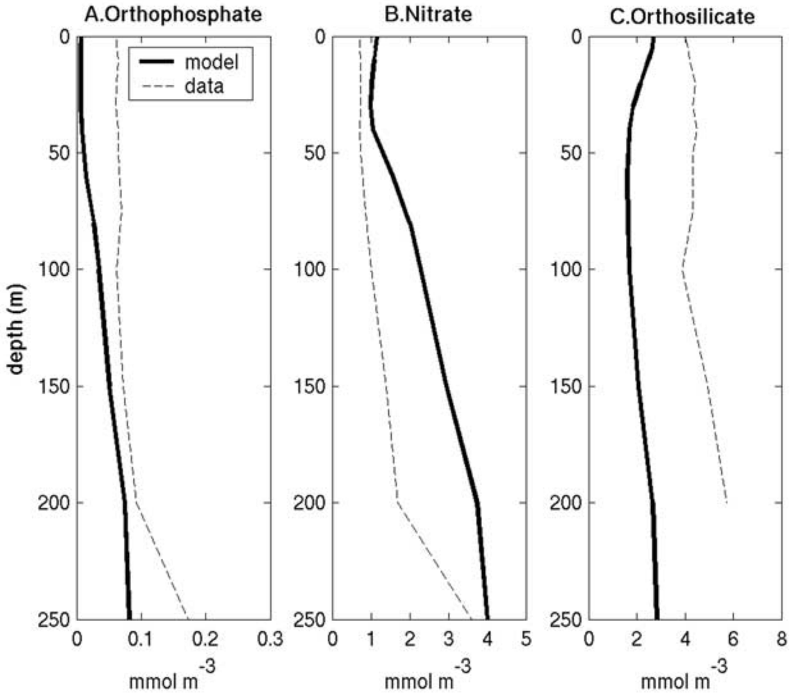

Figure 10. Mean simulated and observed nutrients annual profiles averaged in the central subbasin. (a) Orthophosphate (mmol/m^3); (b) nitrate (mmol/m^3); (c) orthosilicate (mmol/m^3).

the surface, concentrations progressively decrease with depth in all seasons and a chlorophyll *a* subsurface maximum does not develop in summer. Comparison with the ABCD data indicates a general overestimation mainly at surface. Furthermore the observed profiles indicates a roughly constant concentration with depth, contrasting with the depth concentration decrease of the simulated profiles. The chlorophyll *a* overestimation in the surface layer is evident also in the deep northern and the central Adriatic. However, the vertical structure of the profiles and their seasonality shows elements of qualitative agreement with the ABCD observations, notably the development of a

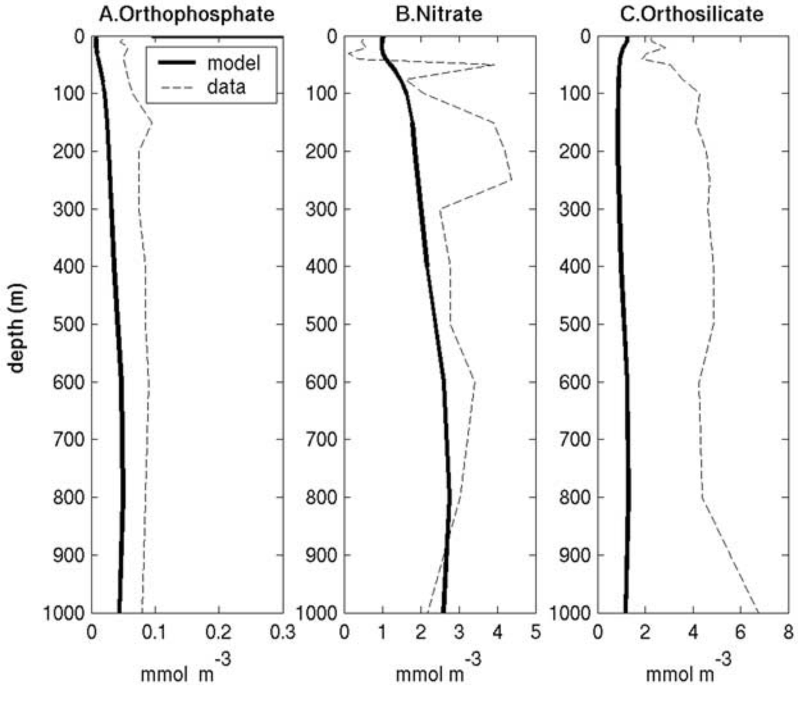

Figure 11. Mean simulated and observed nutrients annual profiles averaged in the southern subbasin. (a) Orthophosphate (mmol/m^3); (b) nitrate (mmol/m^3); (c) orthosilicate (mmol/m^3).

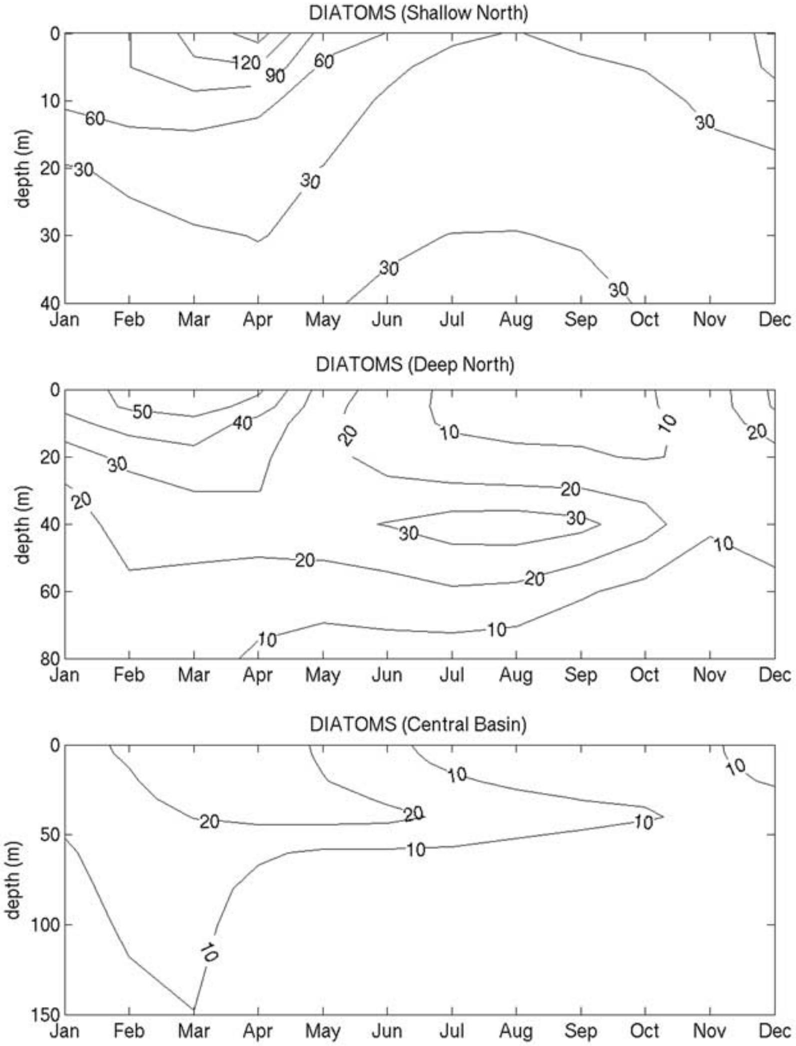

Figure 12. Hovmoller diagrams for diatom functional group annual distribution (mg C/m^3) in the shallow northern, deep northern, and central Adriatic subbasins.

summer subsurface chlorophyll maximum at about 50 m depth in the central Adriatic. This subsurface chlorophyll *a* maximum is also simulated in the deep northern basin, but, the lack of data in this region in the deepest part of the water column, does not allow a comparison. In any case, the general overestimation suggests that the chlorophyll a parameterization in the model still needs further improvements.

4.3. Nutrients

[45] The comparison between simulated annual averaged nutrient profiles and the annual averaged profiles estimated from the ABCD data are shown in Figures 8, 9, 10, and 11. Both data and simulation were averaged in the four Adriatic subbasins. In the shallow northern basin (Figure 8) the surface modeled orthophosphate (Figure 10a) distribution is clearly influenced by the Po river discharge, as the maximum concentrations (0.08 mmol/m^3) are reached in the surface where the simulated values are consistent with the observations. Below a depth of 5 m simulated orthophosphate starts to decrease, reaching, in the deepest part of the water column, values very close to zero, while the observed profile increases with depth, reaching, at 30 m, 0.1 mmol/m^3.

[46] The general shape of the nitrate profile (Figure 8b) is close to that of orthophosphate. The maximum concentration is reached in the upper 10 m of the water column, where the simulated values are close to the observations. Simulated nitrate concentrations progressively decrease with depth and become less than 1 mmol/m^3 below 20 m; conversely, the observed values range between 2 and 3 mmol/m^3 from depth of 20 to 30 m.

[47] Orthosilicate mean profile (Figure 8c) shows a behavior similar to the other nutrients, with higher values in the surface layer and a decrease with depth. Also in this case the model is not able to reproduce the observed nutricline.

[48] In the deep northern basin (Figure 9), the orthophosphate simulated values are permanently lower with respect to the observed data and the model manages, only weakly, to reproduce the nutricline observed starting from 40 m depth.

[49] Simulated nitrate concentrations, on the contrary, are higher than the observations. In the upper layer of the

water column, concentrations are almost constant (around 1 mmol/m^3), while, after 40 m, strongly increase reaching, near the bottom, a value of 2 mmol/m^3. The simulated silicate is higher than the observations in the first 40 m and underestimates the observations in the deeper layer (2 mmol/m^3 against 3.8 mmol/m^3 observed).

[50] In the central basin modeled orthophosphate (Figure 10) is very close to zero in the upper 50 m and increase starting from 50 m reaching, at the bottom, the value of 0.08 mmol/m^3. The values are lower than the observed data, but the shape of the profile is well reproduced. Nitrate-simulated profile also reproduces quite well the shape of the observed one, but, in this case, the simulations are higher than the observations. Modeled orthosilicate ranges from 2 to 4 mmol/m^3 while observed concentrations are always higher than 4 mmol/m^3. The model reproduces the observed weak nutricline starting from 50 m.

[51] In the southern basin all the nutrient-simulated profiles underestimate the observations, but the shape of the profiles is close to those observed. Modeled orthophosphate and nitrate reproduce the weak nutricline present in the observations, while the silicate-simulated profile is almost constant after a depth of 100 m.

[52] Comparison between simulations and observations shows a general model underestimation for orthophosphates and orthosilicates while nitrates are mostly overestimated. The general shape of the observed nutrient profiles is reproduced by the model with the exception of shallow northern basin, where the model does not manage to reproduce the nutrients increase with depth. The overestimation of the phytoplankton biomass, described by the chlorophyll, causing a too strong nutrient uptake, and the low benthic remineralization rate could account for this discrepancy.

4.4. Phytoplankton

[53] Figure 12 shows the modeled diatoms annual cycle (in form of Hovmoller diagrams) averaged in the shallow northern, deep northern and central Adriatic subbasins. The shallow northern basin is characterized by a diatoms bloom during spring (120 mg C/m^3) but high biomass values (30 mg C/m^3) are present all throughout the year. Maximum values are simulated near the surface in all of the seasons.

[54] In the deep northern basin diatom biomass shows a peak in winter (50 mg C/m^3) near the surface. Starting from May diatoms biomass increases with depth and, during the summer, the maximum (30 mg C/m^3) is reached, according to the chlorophyll profiles, at a depth of 40–50 m. The decrease of biomass with respect to the shallow northern basin is evident in all of the seasons.

[55] In the Central basin diatom biomass further decreases with respect to the Northern basin and in summer depicts a subsurface maximum (10 mg C/m^3) at around 50 m.

[56] Figure 13 shows the temporal trend of the modeled ratio between large (>20 μm) and small (<20 μm) phytoplankton biomass (Figure 13a) and of the ratio between simulated bacteria and phytoplankton biomass (Figure 13b) in three different points (A, B and C) subsampled from the model domain (Figure 1). The points are chosen in order to follow the chlorophyll gradient. Point A is located in the most eutrophic area very close to the Po river mouth; point B is in the central area of the northern basin and point C in the southern part of the Adriatic sea where the minimum chlorophyll values are simulated.

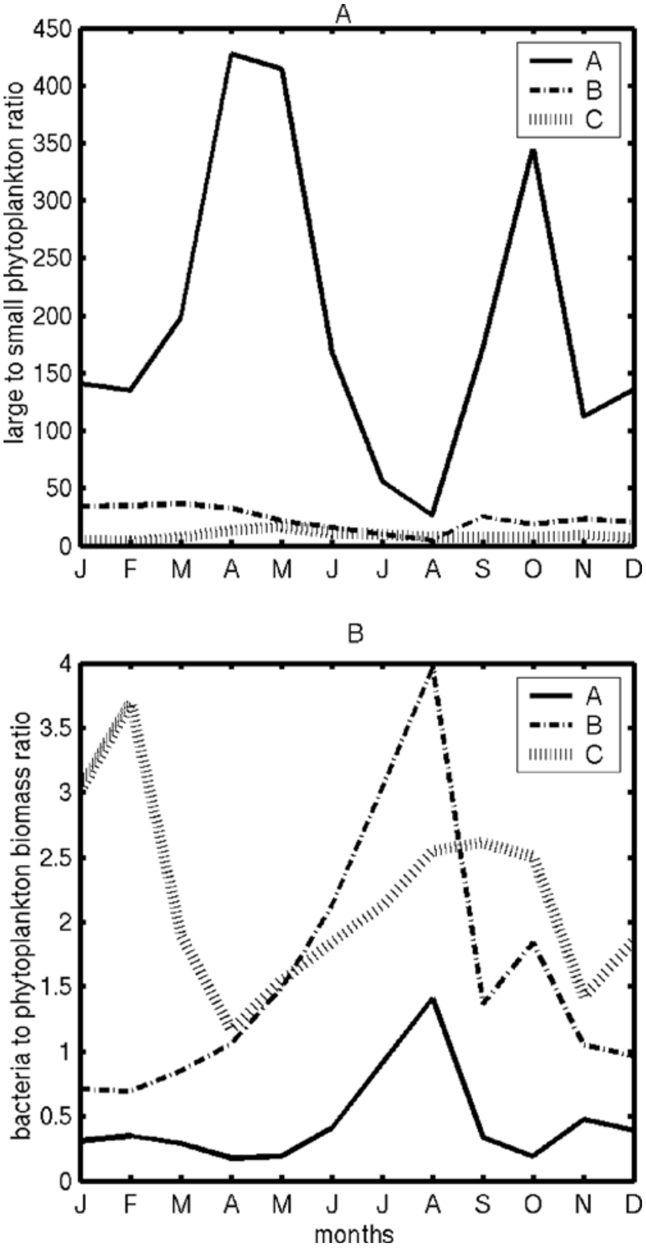

Figure 13. Temporal trend of the ratio (a) between large phytoplankton (>20 μm) and small phytoplankton (<20 μm) and (b) between bacteria and phytoplankton biomass at three points (A, B, and C in Figure 1) subsampled from the model domain.

[57] Large size phytoplankton, supposed to be the diatoms and dinoflagellates (represented by P1 and P4 BFM functional groups, see Appendix A) dominate the system in the three points considered and in every season, as the ratio between large and small phytoplankton is always more than 1. On the other hand the parameter tested shows a strong temporal and space variability ranging from more than 400 at point A, during the winter, to 10 at points B and C during the summer. This behavior implies a wide time and space variability in the phytoplanktonic community composition.

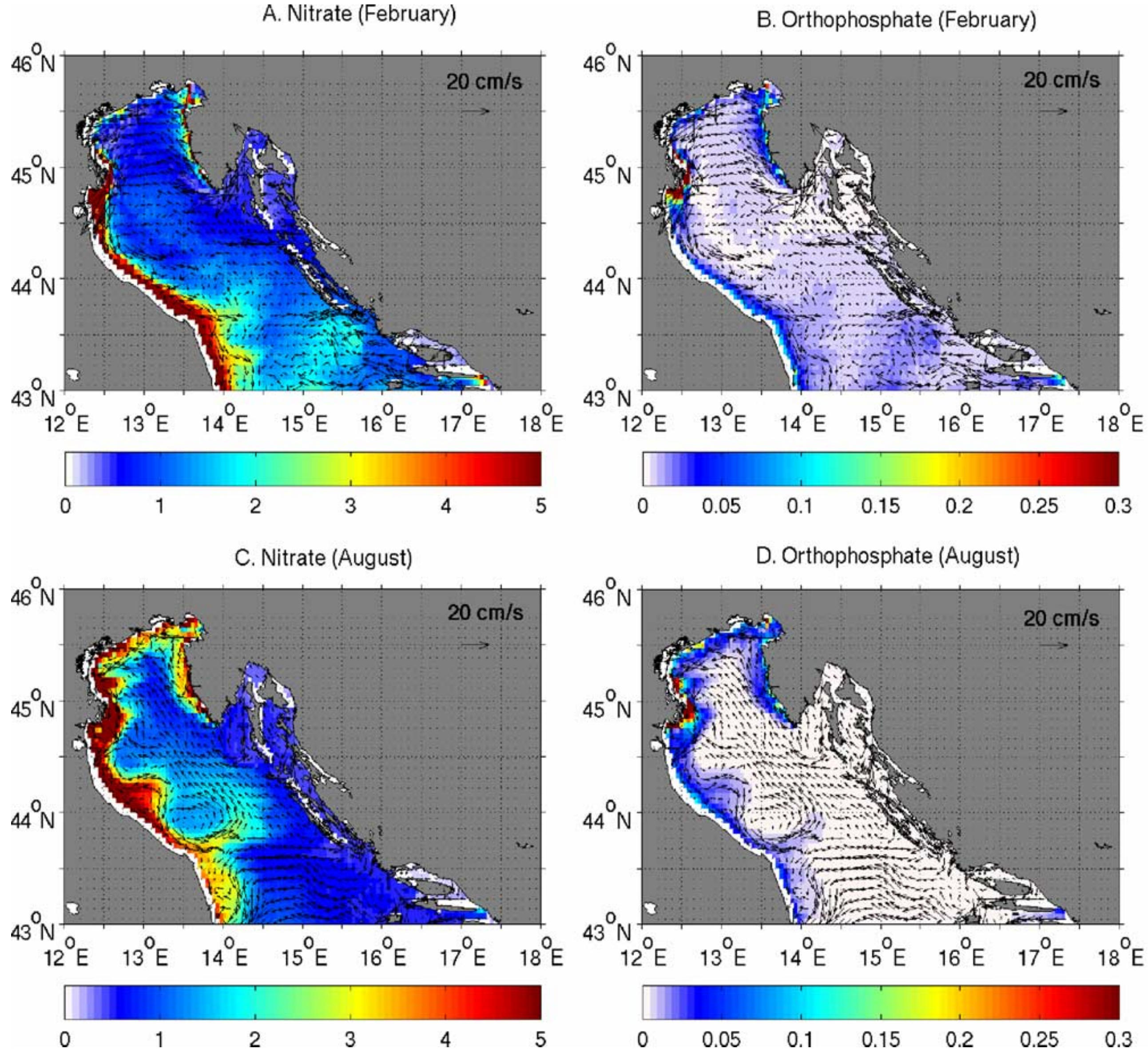

Figure 14. Surface nitrate (mmol/m^3), orthophosphate (mmol/m^3), and velocity fields (cm/s) monthly averages in the northern basin. (a and b) February and (c and d) August.

[58] In particular the gradient between point A and B is connected to the inshore and the offshore regimes of the WACC. A much larger proportion of large cells is present in the onshore regime and the offshore of the WACC in the northern Adriatic is similar to the community composition in the southern Adriatic, i.e., a fully oligotrophic regime. This large gradient, next to the Po river mouth, magnifies the connection between the physical regimes and the primary producer biomasses.

[59] The ratio between bacteria and phytoplankton biomass is always less than 1 at point A, implying eutrophic conditions [*Thingstad and Rassoulzadegan*, 1999]. Only in summer do phytoplankton biomass become comparable to those of bacteria. At point B the ratio between bacteria and phytoplankton biomass is around 1 during winter and autumn while, in spring and summer, it increases reaching the value of 4.5. This behavior implies a strong seasonal variability in terms of planktonic community composition. At point C modeled bacteria always dominate the system as the bacteria to phytoplankton ratio ranges from 1 (in spring) to 3.5 in winter.

[60] This analysis indicates the shift of the planktonic community between an eutrophic large-size species dominated regime onshore to the WACC, and a more oligotrophic system offshore of the WACC and in the southern Adriatic, in which the small size phytoplankton and bacteria become dominant. The model is thus capable of reproducing different trophic conditions not only in terms of biomass amount, but also in terms of planktonic community structure due to different physical conditions that shift the system from a nutrient (offshore) to a light (onshore) limited regime.

4.5. Coupling Between Physical Processes (WACC) and Biogeochemical Variables

[61] Figure 14 shows the surface distributions of nitrate and orthophosphate and the velocity fields, averaged for

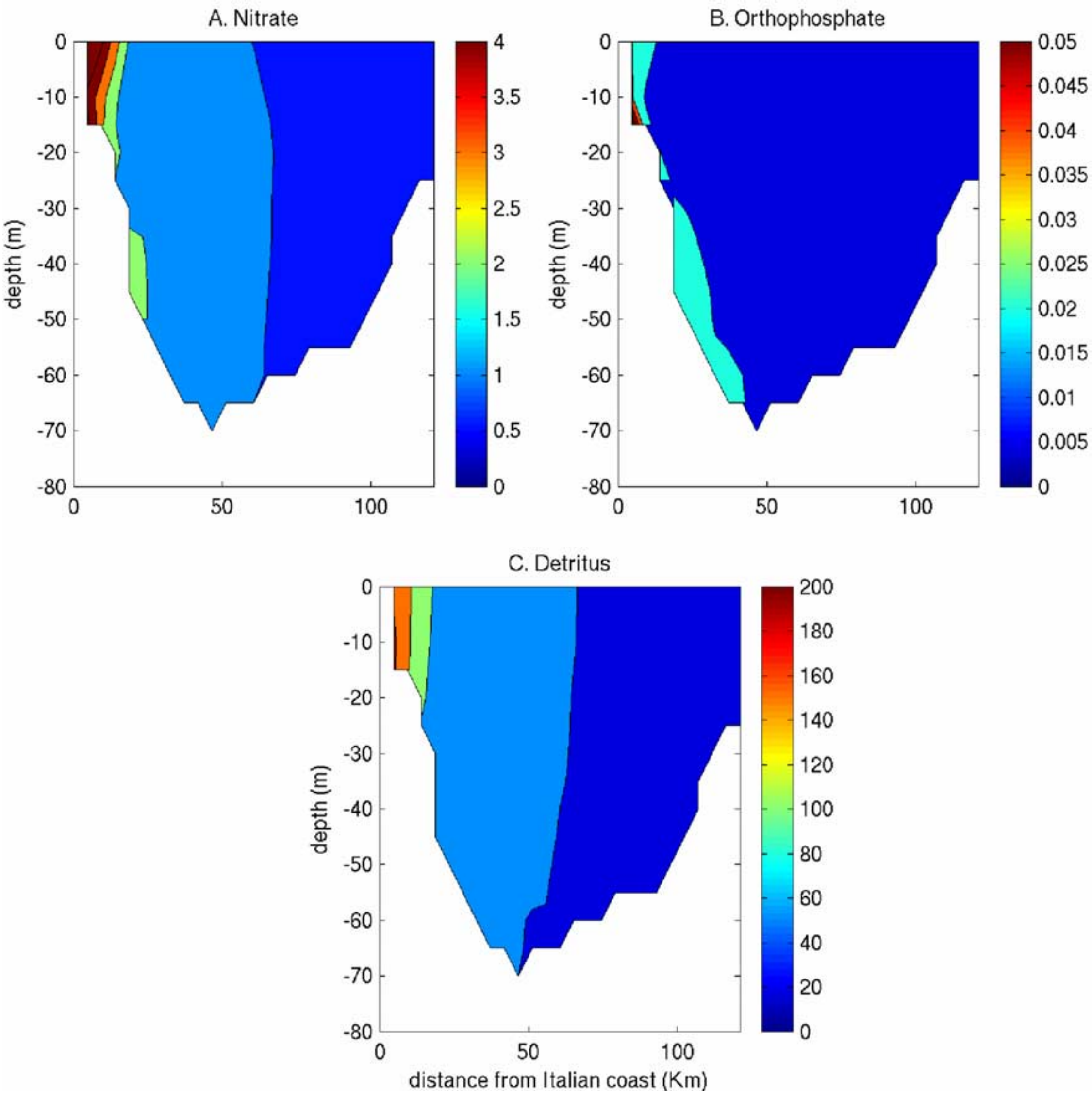

Figure 15. (a) Nitrate (mmol/m^3), (b) orthophosphate (mmol/m^3), and (c) particulate detritus (mg C/m^3) averaged on cross section A indicated in Figure 1. Data are averaged for February.

February (Figures 14a and 14b) and August (Figures 14c and 14d) in the northern Adriatic Sea. The Adriatic Western Coastal Current (WACC) is clearly reproduced by the model both in February and August, and the distribution of nutrients appear clearly related to this circulation phenomena. The WACC is closer to the coastal boundary of the model (supposed to be at a depth of 10 m depth) during winter, while it is meandering during summer. This affects the transport of nutrients farthest offshore during summer than in winter, as can be seen from Figure 14c for nitrates.

[62] The simulated nitrate, in February, reaches the maximum values in a restricted area close to the Italian coast and is transported by the WACC toward the southern part of the basin. In this way high nitrate concentrations reach the central Adriatic basin. A very low nitrate concentration is present in the offshore area and a very steep coastal–offshore area gradient is depicted by the model.

[63] Orthophosphate distribution presents high concentration (more than 0.3 mmol/m^3) only in correspondence of the river sources and the transport along the WACC is very weak. This implies that orthophosphate is very quickly consumed by primary producers and bacteria in the area close to the river mouths. The first conclusion from this work is that the frontal structure of the WACC provides a means to create a frontal structure also for biochemical state variables that are not limiting.

[64] The discrepancy between the behavior of nitrate and orthophosphate is, in fact, due to the Adriatic P limitation, present in the model as the N/P ratio in the nutrient river loading is 40. As for the nitrate, the central area of the basin is phosphorus depleted both in February and in August.

[65] The role of the WACC in determining nutrient and chlorophyll (primary producers) fate and distribution is also evident from the analysis of the simulated concentration of nitrate, orthophosphate and organic particulate detritus interpolated on the cross section A (see Figure 1) shown in Figure 15. Simulated values were averaged for February. High nitrate and orthophosphate concentrations are restricted

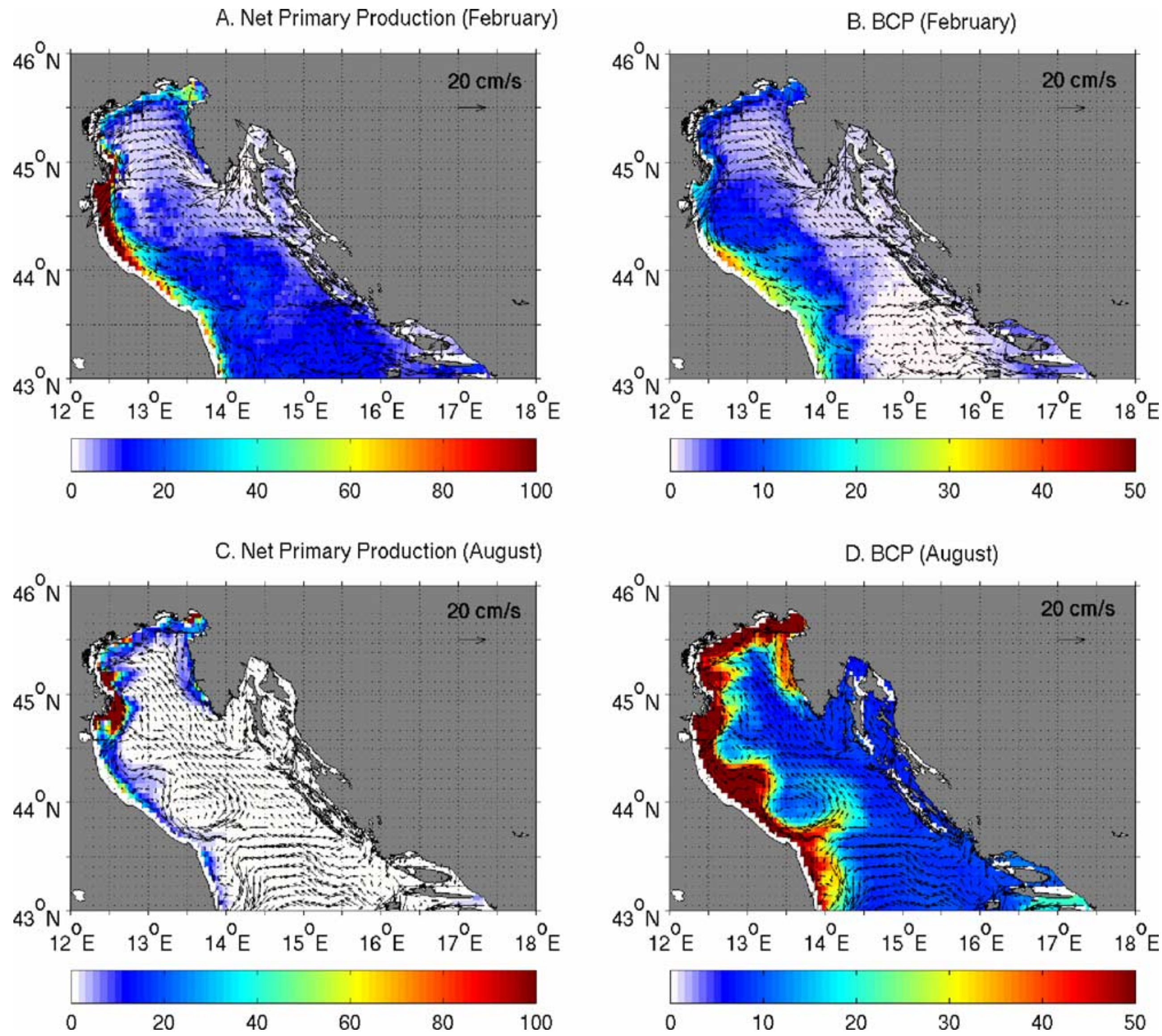

Figure 16. Surface net primary production (mg C m^{-3} d^{-1}), bacterial carbon production (BCP, mg C m^{-3} d^{-1}), and velocity field (cm/s) monthly averages in the northern basin. (a and b) February and (c and d) August.

to the first 20 km off the Italian coast. As already pointed out by the horizontal map, at this latitude, near the western coast, the nitrate concentration is close to that simulated in the surface near the Po river mouth, while the orthophosphate is remarkably lower as it is the limiting nutrient and, consequently, is very quickly depleted. In the central and eastern part of the section concentrations of both nitrate and orthophosphate are very close to zero. The particulate detritus is present, in a significant concentration (more than 100 mg C/m^3) only along the Italian coast and tends to be very low (less than 40 mg C/m^3) in the offshore area starting 40 km off the Italian coast.

4.6. Primary and Bacterial Production

[66] The simulated surface net primary production (Figure 16) shows high values along the Italian coast in February (Figure 16a), while in August (Figure 16c), such high values are simulated only near the nutrient sources, mainly the Po river mouth. This implies that during winter along the Emilia Romagna coastal area there is in situ high primary production. Conversely, in summer, the conditions for an high productivity are restricted to a limited area near the nutrient supplies (mainly the Po river mouth) and we argue that the high chlorophyll concentrations, described by the remote sensing data, in summer along the Emilia-Romagna coasts and further south (Figure 6), are related to the advective and diffusive processes due to the WACC and not to a local production.

[67] The difference between the primary production distribution in February and August can be explained by the role of bacterioplankton activity and, consequently, by the semi-labile dissolved organic carbon (DOC) cycle. Figures 16b and 16d shows the simulated surface bacterial carbon production (BCP) averaged for February and August in the northern basin. The BCP is low in February (from 0 to 30 mg C m^{-3} d^{-1}), while, is much higher in August,

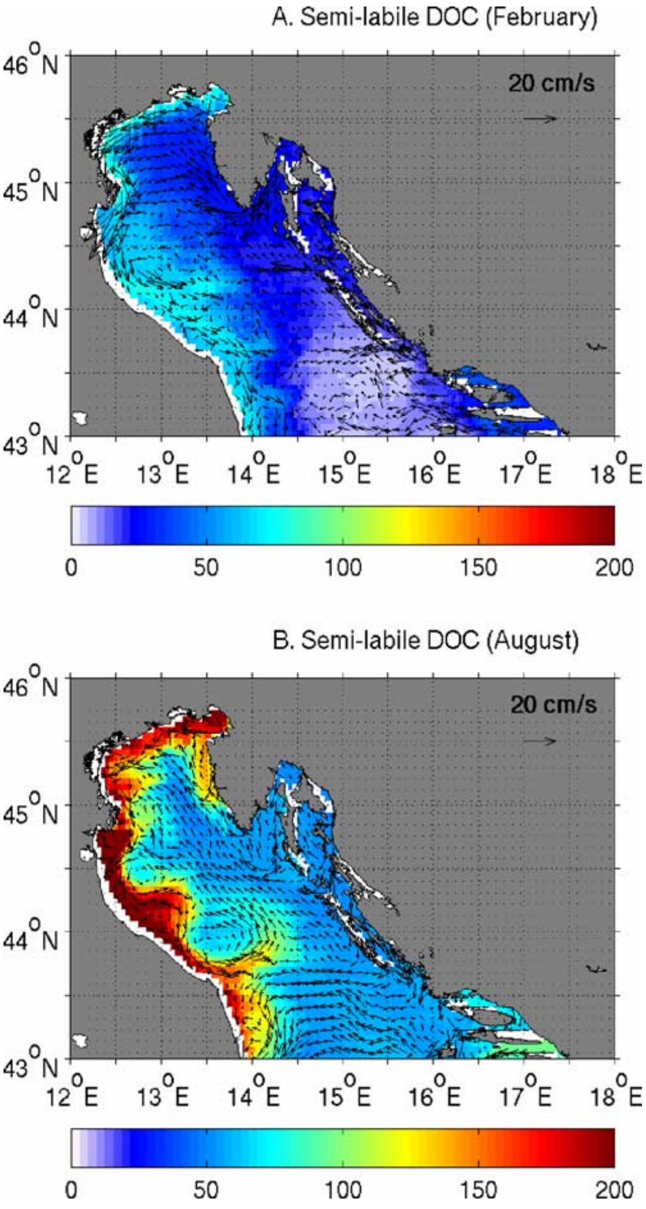

Figure 17. Surface semilabile dissolved organic carbon (DOC) (mmol/m^3) and velocity field (cm/s) monthly averages in the northern basin. (a) February and (b) August.

(from 1 to 60 mg C m^{-3} d^{-1}). The bacteria activity is thus decoupled from the primary production. Figure 17 shows the surface concentrations of the semilabile DOC averaged for February and August. This class of DOC is mainly produced by phytoplankton activity and is the main substrate for the bacterial growth [*Polimene et al.*, 2006]. Low BCP, simulated in February, is related to low semilabile DOC concentrations (Figure 17a) while high BCP simulated in August is a consequence of high semilabile DOC concentrations (Figure 16b). As already suggested by zero-dimensional modeling experiments [*Polimene et al.*, 2006] the presence of a large amount of semilabile DOC, inducing a strong bacterial uptake of the limiting nutrient, limits phytoplankton growth. Starting from this assumption model simulations suggest the following seasonal succession between phytoplankton, DOC and bacteria: during winter, high riverine nutrients discharge induces phytoplankton blooms; in this season phytoplankton dominates the system because the poor DOC pool (Figure 17a) does not induce any competition between bacteria and phytoplankton for nutrients. Conversely, in summer, high DOC concentrations (mostly the semilabile fraction) generated by primary producers induce strong nutrients uptake by bacteria which outcompete phytoplankton and dominate the system. Primary production is then restricted in a zone very close to the nutrients input where nitrate and orthophosphate concentrations are so high to sustain both bacterial and phytoplanktonic growth.

5. Conclusions and Future Work

[68] This first simulation of the Adriatic Sea ecosystem seasonal variability with a fully three-dimensional ecosystem model and a realistic basin geometry has been shown and discussed.

[69] For the first time, a coupled physical and biogeochemical model was used to simulate at about 5 km resolution the whole Adriatic Sea primary production cycle and results were validated against SeaWiFS data and historical in situ data.

[70] Our results reproduce some of the main characteristics of the Adriatic Sea biogeochemistry connected to the large-scale east-west and north-south gradients. These results are in agreement with previous idealized numerical studies by *Zavatarelli et al.* [2000] which however were not able to resolve the structures of the primary producers distributions. Their simulations in fact could not resolve the WACC intensified chlorophyll front down almost to the Otranto Strait.

[71] In particular the seasonal chlorophyll variability is qualitatively captured by the model in comparison with SeaWiFS data. The comparison with the ABCD data also shows that the basic assumptions of the model are reasonable.

[72] Despite the correct simulation of some features, the model still has many weak points. The overestimation of chlorophyll concentration suggests the need for an improvement of the nutrient discharge parameterizations. In addition, the simple benthic return model used in this study is certainly not able to reproduce the complexity of the water column–sediment interactions, therefore the introduction of a full benthic model would enhance the processes occurring on the bottom layer improving the simulation of the deep water column nutrients.

[73] Even with all these limitations, the model gives qualitative information about the ecosystem seasonal cycle of the Adriatic basin. The simulations highlight the coupling between circulation structures and biogeochemical variables indicating that the WACC frontal area, corresponding to a temperature and salinity front [*Zavatarelli and Pinardi*, 2003], produces an ecosystem front. This front separates a large phytoplankton and relatively small bacterial biomass region from the offshore area where the ecosystem dynamics is similar to the one of the southern Adriatic which is a completely oligotrophic area.

[74] Our results indicate that the shift of the carbon flux between a bacterial dominated food web and an herbivorous

one described by *Thingstad and Rassoulzadegan* [1999] can occur, spatially, in few tens of kilometers, and, temporally, at the seasonal timescale.

Appendix A: BFM Primary Producers Parameterization

[75] Primary producers in the BFM are divided in four functional group by means of which is possible, on a first approximation, reproduce the functionality of phytoplankton in marine ecosystem.

[76] The operational model definition of the phytoplankton functional types are (1) diatoms (functional group P1), unicellular eukaryotes enclosed by silica frustule eaten by micro and mesozooplankton; (2) autotrophic nanoflagellates (functional group P2), dimension 2–20 μm, motile unicellular eukaryotes comprising smaller dinoflagellates and other autotrophic nanoplankton flagellates eaten by heterotrophic nanoflagellates, microzooplankton and mesozooplankton; (3) Picophytoplankton (functional group P3), dimension 0.2–2 μm, smallest autotrophic unicellular organism grazed by heterotrophyc nanoflagellates, with an almost total preferential use of ammonium nitrogen instead of other nitrogen species; and (4) inedible or partially inedible phytoplankton (functional group P4), dimension 20–200 μm, that represent a wide group of phytoplanktonic species also comprising larger species belonging to the previous groups but also those that during some period of the year develop a form of (chemo) defense to predator attack. This group generally has low growth rates and small or zero food matrix elements with respect to micro and mesozooplankton groups.

A1. Phytoplankton Environmental Regulating Factors

[77] The physiological regulating factors for the phytoplankton groups contain the functional response of the organism to environmental conditions such temperature, light, and inorganic nutrients availability. The net growth rate of phytoplankton depends mainly on light, temperature, nutrient availability, and, according to *Droop* [1973] and *Nyholm* [1977], the internal nutrient storage. In order to account for the environmental and intracellular conditions in the parameterized functional response of phytoplankton, a set of a non dimensional regulating factor are also included in the mathematical formulation. As a general rule, the value of a regulating factor is 1, under optimum conditions, and tends to 0 when organisms are limited by one of the environmental limiting factor.

A1.1. Temperature

[78] The dependence of the physiological regulating factor from environmental water temperature T is common to all the parameterizations of the functional groups and of many other biogeochemical processes It is written in an exponential forms as

$$f^T = Q_{10}^{\frac{T-T_0}{T_0}} \quad T_0 = 10^o C \tag{A1}$$

In the case of phytoplankton, Q_{10} is set to 2 for all the group, indicating that the potential growth rate doubles every 10°C This is the only regulating factor that can give a value larger than 1.

A1.2. Light Regulating Factor

[79] The light regulating factor is formulated as:

$$f_P^I = \min\left(1, I_{PAR}/I_P^{opt}\right) \tag{A2}$$

where I_{PAR} is the photosynthetically available radiation (PAR), and I_P^{opt} t is the optimal light computed according to *Ebenhöh et al.* [1997]. I_{PAR} derive from the shortwave irradiance term given by the physical model taking in to account the extinction due to suspended particles. The irradiance used as forcing function for the calculation of production rates is written as:

$$I_{PAR} = \varepsilon_{PAR} Q_S e^{(\lambda_\nu + \lambda_{bio})z} \tag{A3}$$

where ε_{PAR} is the coefficient determining the portion of PAR (usually 0.5), λ_ν is the background extinction coefficient of the water and

$$\lambda_{bio} = \sum_j c_{P^{(j)}} P_c^{(j)} + c_{R^{(6)}} R6c + c_{ISM} ISM \tag{A4}$$

is the extinction coefficient due to phytoplankton, particulate detritus and suspended inorganic matter. The different C factor represent the specific fraction to the total extinction coefficient of each suspended substance. P_c^j is the phytoplankton carbon biomass where the subscript j = (1,2,3,4) indicate the four phytoplankton functional group described below. *R6c* is the particulate organic detritus and *ISM* is the inorganic suspended material.

A1.3. Nutrient Regulating Factor

[80] The nutrients uptake processes in phytoplankton are decoupled from the photosynthetic carbon assimilation process. The basic idea of the decoupling is that the Redfield ratio [*Redfield et al.*, 1963] is considered as the threshold value between a nutrient-limiting and nonlimiting situation, and that the intracellular varying nutrient/carbon quota in phytoplankton always vary within a fixed range around a fixed threshold. The Redfield ratio ($R_{r_c^{n,p}}$) values are introduced in the model equations as a constant parameters.

[81] According to the value given by *Sommer* [1994], it is assumed that the minimum quota for nitrogen and phosphorus correspond to the nutrient content of the structural parts of the cell and are taken to be half the Redfield ratio as follows:

$$n_P^{\min} = \frac{Rr_c^n}{2},\ p_P^{\min} = \frac{Rr_c^p}{2}. \tag{A5}$$

The maximum value are the maximum storage capacity of phosphorus and nitrogen with respect to carbon, taken to be twice the Redfield ratio:

$$n_P^{\max} = 2Rr_c^n,\ p_P^{\max} = 2Rr_c^p \tag{A6}$$

[82] The minimum quota are used in conjunction with Redfield ratio for determining the internal nutrient status of cells. The regulating factor for the nutrient limitation

depends on the difference between the minimum reference value and the actual dynamical internal quota as

$$f_P^n = \min\left(1, \max\left(0, \frac{P_n/P_c - n_P^{\min}}{Rr^n - n_P^{\min}}\right)\right) \tag{A7}$$

$$f_P^p = \min\left(1, \max\left(0, \frac{P_p/P_c - p_P^{\min}}{Rr^p - p_P^{\min}}\right)\right) \tag{A8}$$

In order to make the decoupling effective, these non dimensional parameters are only applied to the carbon loss terms and not to the assimilation of CO_2 trough the photosynthesis.

[83] Concerning the silica dynamics it remains coupled to the uptake of inorganic carbon. This difference with respect to the others nutrients is due to the lack of internal storage capacity for silica in diatoms. A Michaelis-Menten function controls the regulating factor for silica:

$$f_{P(1)}^S = \frac{N5}{N5 + h_{P(1)}^S} \tag{A9}$$

This is function of the external silica concentration ($N5$), where $h_{P(1)}^S$ is the half saturation constant of silicate concentration in the water.

[84] The combined effect of the regulating factors for nutrient limitation is parameterized applying the Liebig principle of the most limiting nutrient, in the following form:

$$f_P^{n,p} = \min\left(f_P^p, f_P^n\right) \qquad f_{P(1)}^{n,p,s} = \min\left(f_{P(1)}^{n,p}, f_{P(1)}^s\right) \tag{A10}$$

A2. Mathematical Formulation of the Biogeochemical Processes

[85] The biological source terms solved in the BFM for the primary producers are: gross primary production (gpp), respiration (rsp), exudation (exu), cell lysis (lys) and predation (prd). As detailed by *Vichi et al.* [2004] and *Blackford et al.* [2004], there is an equation for any internal component of a generic phytoplankton group $P(c, n, p, s)$. The equations are written in the form $\frac{\partial A}{\partial t}\Big|_Y^X$ where A is the state variable X is the process described and Y the state variables or the functional group involved in the process [*Vichi et al.*, 2004]:

$$\left.\frac{\partial P_c}{\partial t}\right|_{bio} = \left.\frac{\partial P_c}{\partial t}\right|_{O3}^{gpp} - \left.\frac{\partial P_c}{\partial t}\right|_{O3}^{rsp} - \left.\frac{\partial P_c}{\partial t}\right|_{R2c}^{exu} - \left.\frac{\partial P_c}{\partial t}\right|_{R1c}^{lys} - \left.\frac{\partial P_c}{\partial t}\right|_{R6c}^{lys} - \sum_j \left.\frac{\partial P_c}{\partial t}\right|_{Zc}^{prd} \tag{A11}$$

$$\left.\frac{\partial P_n}{\partial t}\right|_{bio} = \left.\frac{\partial P_n}{\partial t}\right|_{N3,N4}^{upt} - \left.\frac{\partial P_n}{\partial t}\right|_{R1n}^{lys} - \left.\frac{\partial P_n}{\partial t}\right|_{R6n}^{lys} - \frac{P_n}{P_c}\sum_j \left.\frac{\partial P_c}{\partial t}\right|_{Zc}^{prd} \tag{A12}$$

$$\left.\frac{\partial P_p}{\partial t}\right|_{bio} = \left.\frac{\partial P_p}{\partial t}\right|_{N1p}^{upt} - \left.\frac{\partial P_p}{\partial t}\right|_{R1n}^{lys} - \left.\frac{\partial P_p}{\partial t}\right|_{R6p}^{lys} - \frac{P_p}{P_c}\sum_j \left.\frac{\partial P_c}{\partial t}\right|_{Zc}^{prd} \tag{A13}$$

$$\left.\frac{\partial P_s}{\partial t}\right|_{bio} = \left.\frac{\partial P_s}{\partial t}\right|_{N5}^{upt} - \left.\frac{\partial P_s}{\partial t}\right|_{R6s}^{lys} - \frac{P_s}{P_c}\sum_j \left.\frac{\partial P_c}{\partial t}\right|_{Zc}^{prd} \tag{A14}$$

Equation (A14) describing the rate of change of the cellular silica content, is included only in the diatoms (P1) parameterization. The subscript terms are defined as follow: $O3$, carbon dioxide; $R2c$, semilabile dissolved organic carbon; $R1c$, labile dissolved organic carbon; $R1n$,dissolved organic nitrogen; $R1p$, dissolved organic phosphorus; $R6c$, particulate organic carbon; $R6p$, particulate organic phosphorus; $R6n$, particulate organic nitrogen; $R6s$, particulate organic silica; $N1p$, phosphate, $N3$, nitrate; $N4$, ammonium; $N5$, silica; Zc, zooplankton carbon biomass.

A3. Carbon Dynamics

[86] Gross primary production is a function of the environmental regulating factors, the potential photosynthetic rate r_{0p} and the phytoplankton biomass.

$$\left.\frac{\partial P_c}{\partial t}\right|_{O3}^{gpp} = f_p^T f_p^I r_{0p} P_c \tag{A15}$$

The exudation term is controlled by the internal nutrients ratio and is modulated by the constant fraction of activity excretion α_p:

$$\left.\frac{\partial P_c}{\partial t}\right|_{R2c}^{exu} = \left[\alpha_p + \left(1 - \alpha_p\right)\left(1 - f_p^{n,p}\right)\right] \left.\frac{\partial P_c}{\partial t}\right|_{O3}^{gpp} \tag{A16}$$

The lysis of cells is supposed to generate both dissolved and particulate detritus. The percentage going to dissolved detritus is inversely proportional to the internal nutrient content. The portion of the cellular material that go in to the particulate organic carbon is

$$\left.\frac{\partial P_c}{\partial t}\right|_{R6c}^{lys} = \varepsilon_p^{n,p} \frac{h_p^{p,n,s}}{f_p^{p,n,s} + h_p^{p,n,s}} d_{0p} P_c \tag{A17}$$

The parameter d_{0p} is the constant specific potential lysis rate and $h_p^{p,n,s}$ is the half-saturation constant. The portion of cell lysis directed to the dissolved detritus is then

$$\left.\frac{\partial P_c}{\partial t}\right|_{R1c}^{lys} = \left(1 - \varepsilon_p^{n,p}\right) \frac{h_p^{p,n,s}}{f_p^{p,n,s} + h_p^{p,n,s}} d_{0p} P_c \tag{A18}$$

The term $\varepsilon_p^{n,p}$ present in the equations (A17) and (A18) is given by

$$\varepsilon_p^{n,p} = \min\left(1, \frac{p_p^{\min}}{P_p/P_c}, \frac{n_p^{\min}}{P_n/P_c}\right) \tag{A19}$$

The respiration term is defined as the sum of the basal respiration and the activity respiration

$$\left.\frac{\partial P_c}{\partial t}\right|_{O3}^{rsp} = f_p^T b_p P_c + \gamma_p \left\{ \left.\frac{\partial P_c}{\partial t}\right|_{O3}^{gpp} - \left.\frac{\partial P_c}{\partial t}\right|_{R2c}^{exu} \right\} \tag{A20}$$

b_p is the constant specific respiration rate and γ_p is the fraction of primary production respirated.

[87] The grazing loss term due to zooplankton activity is supposed to be dependent on the temperature, zooplankton and phytoplankton biomass:

$$\left.\frac{\partial P_c}{\partial t}\right|_{Z}^{prd} = f^T z_{oz} \frac{P_c}{P_c + h_z} Z_c \tag{A21}$$

where ro_z is the maximum specific daily ingestion rate and h_z is the half saturation constant for the food.

A4. Nitrogen and Phosphorus Dynamics

[88] Nitrogen and phosphorus dynamics are parameterized in the same way then only the case of phosphorus is described. The uptake is thought to be a combination of two different rate of uptake; u_p^{ext} dependent on the external nutrient concentration and u_p^{int} dependent on the internal nutrients quota, according to the kinetics described by *Droop* [1973]. The phosphorus uptake is then written as:

$$\left.\frac{\partial P_p}{\partial t}\right|_{N1p}^{upt} = \min\left(u_p^{ext}, u_p^{\text{int}}\right) P_c \tag{A22}$$

where

$$u_p^{ext} = \lambda_1^{ext} N1_p \tag{A23}$$

and

$$u_p^{\text{int}} = g_p p_p^{\max} + \nu_p \left[p_p^{\max} - \frac{P_p}{P_c}\right] \tag{A24}$$

λ_1^{ext} represent the specific membrane affinity for orthophosphate and g_p is the net specific carbon growth rate, obtained from equation (A11) and defined as

$$g_p = \frac{1}{P_c}\left(\left.\frac{\partial P_c}{\partial t}\right|_{O3}^{gpp} - \left.\frac{\partial P_c}{\partial t}\right|_{O3}^{resp} - \left.\frac{\partial P_c}{\partial t}\right|_{R2c}^{exu} - \left.\frac{\partial P_c}{\partial t}\right|_{R6c}^{lys} - \left.\frac{\partial P_c}{\partial t}\right|_{R1c}^{lys}\right) \tag{A25}$$

The lysis processes affects phytoplankton nutrient content exactly as the carbon content. The death cell material is directed into particulate organic phosphorus *R*6*p*:

$$\left.\frac{\partial P_p}{\partial t}\right|_{R6p}^{lys} = P_p^{\min} \left.\frac{\partial P_c}{\partial t}\right|_{R6c}^{lys} \tag{A26}$$

Also, in dissolved organic phosphorus *R*1*p*:

$$\left.\frac{\partial P_p}{\partial t}\right|_{R1p}^{lys} = \frac{h_p^{p,n,s}}{f_p^{p,n,s} + h_p^{p,n,s}} d_{0p} - \left.\frac{\partial P_p}{\partial t}\right|_{R6p}^{lys} \tag{A27}$$

The loss term due to the predation are written in the form

$$\left.\frac{\partial P_p}{\partial t}\right|_{Zp}^{prd} = \frac{P_p}{P_c} \left.\frac{\partial P_c}{\partial t}\right|_{Zc}^{prd} \tag{A28}$$

A5. Silica Dynamics

[89] For the Silica dynamics there is no internal storage, therefore the uptake is supposed to be directly dependent on the net specific carbon growth rate g_p taking into account the Si:C reference ratio Rr_c^s as follow:

$$\left.\frac{\partial P_s}{\partial t}\right|_{N^5}^{lys} = g_p Rr_c^s P_c \tag{A29}$$

Silicate is released only in particulate form, because it is incorporated in the diatom theca. The loss term of particulate silicate due to lysis processes is written as

$$\left.\frac{\partial P_s}{\partial t}\right|_{R6s}^{lys} = \frac{P_s}{P_c} \left.\frac{\partial P_c}{\partial t}\right|_{R1c,R6c}^{lys} \tag{A30}$$

Since zooplankton do not have a silica component, the loss term due to the predation is transferred to the particulate organic silica *R*6*s*:

$$\left.\frac{\partial P_s}{\partial t}\right|_{R6s}^{prd} = \frac{P_s}{P_c} \left.\frac{\partial P_c}{\partial t}\right|_{Zc}^{prd} \tag{A31}$$

[90] **Acknowledgments.** The leading author of this paper was supported by a Ph.D. fellowship given to the Environmental Science graduate program of the University of Bologna at Ravenna and by the CNR-ISMAR (Istituto di Scienze Marine) of Bologna. The other two authors (N. Pinardi and M. Zavatarelli) were partially supported by the MFSTEP project (EU contract EVK3-CT-2002-00075). Marcello Vichi is greatly acknowledged for help in setting up the version of the BFM numerical code.

References

Artegiani, A., D. Bregant, E. Paschini, N. Pinardi, F. Raicich, and A. Russo (1997a), The Adriatic Sea general circulation. Part I: Air sea interactions and water mass structure, *J. Phys. Oceanogr.*, *27*, 1492–1514.

Artegiani, A., D. Bregant, E. Paschini, N. Pinardi, F. Raicich, and A. Russo (1997b), The Adriatic Sea general circulation. Part II: Baroclinic circulation structure, *J. Phys. Oceanogr.*, *27*, 1515–1532.

Baretta, J. W., W. Ebenhoh, and P. Ruardij (1995), The European Regional Seas Ecosystem Model, a complex marine ecosystem model, *Neth. J. Sea Res.*, *33*, 233–246.

Blackford, J. C., J. I. Allen, and F. J. Gilbert (2004), Ecosystem dynamics at six contrasting sites: A generic modelling study, *J. Mar. Syst.*, *52*, 191–215.

Degobbis, D., and M. Gilmartin (1990), Nitrogen, phosphorus and biogenic silicon budgets for the northern Adriatic Sea, *Oceanol. Acta*, *13*, 31–45.

Degobbis, D., M. Gilmartin, and N. Revelante (1986), An annotated nitrogen budget calculation for the northern Adriatic Sea, *Mar. Chem.*, *20*, 159–177.

Droop, M. R. (1973), Some thoughts on nutrient limitation in algae, *J. Phycol.*, *9*, 264–272.

Ebenhöh, W., J. Baretta, and J. Baretta (1997), The primary production module in the marine ecosystem model ERSEM II with emphasis on the light forcing, *J. Sea Res.*, *38*, 173–193.

Franco, P. (1984), Fattori influenti sulla produttività primaria dell'Adriatico settentrionale, *Boll. Oceanol. Teorica Appl.*, *2*, 125–140.

Giani, M., F. Savelli, D. Berto, V. Zangrando, B. Ćosović, and V. Vojvodić (2005), Temporal dynamic of dissolved and particulate organic carbon in the northern Adriatic Sea in relation to the mucilage events, *Sci. Total Environ.*, *353*, 232–246.

Gilmartin, M., D. Degobbis, N. Relevante, and N. Smodlaka (1990), The mechanisms controlling plant nutrient concentration in the northern Adriatic Sea, *Int. Rev. Ges. Hydrobiol.*, *75*, 425–445.

Maggiore, A., M. Zavaterelli, M. G. Angelucci, and N. Pinardi (1998), Surface heat and water fluxes in the Adriatic Sea: Seasonal and interannual variability, *Phys. Chem. Earth.*, *23*, 561–567.

Nyholm, N. (1977), Kinetics of nitrogen-limited algal growth, *Prog. Water Technol.*, *8*, 347–358.

O'Reilly, J. E., et al. (2000), Ocean color chlorophyll *a* algorithms for SeaWiFS, OC2, and OC4: version 4, in *SeaWiFS Postlaunch Calibration and Validation Analyses, Part 3*, vol. 11, edited by S. B. Hooker and E. R. Firestone, *NASA Tech. Memo.*, *2000–206892*, 49 pp.

Polimene, L., J. I. Allen, and M. Zavatarelli (2006), Model of interactions between dissolved organic carbon and bacteria in marine systems, *Adv. Microbiol. Ecol.*, *43*, 127–138.

Provini, A., G. Crosa, and R. Marchetti (1992), Nutrient export from the Po and Adige river basin over the last 20 years, in *Marine Coastal Eutrophication*, edited by R. A. Vollenweider, R. Marchetti, and R. Viviani, pp. 291–313. Elsevier, New York.

Raicich, F. (1994), Note on the flow rates of the Adriatic Rivers, *Tech. Rep. RF-02/94*, 8 pp., Ist. Sper. Talassografico, Trieste, Italy.

Raicich, F. (1996), A study of the freshwater balance of the Adriatic Sea, *J. Mar. Syst.*, *9*, 305–319.

Redfield, A. C., B. Ketchum, and F. Richards (1963), The influence of organisms on the composition of sea water, in *The Sea*, edited by M. Hill, pp. 26–77, Wiley-Interscience, Hoboken, N. J.

Revelante, N., and M. Gilmartin (1992), The lateral advection of particulate organic matter from the Po delta region during summer stratification and its implication for the northern Adriatic, *Estuarine Coastal Shelf Sci.*, *35*, 191–212.

Simpson, J. H. (1997), Physical processes in the ROFI regime, *J. Mar. Syst.*, *12*, 3–15.

Smodlaka, N. (1986), Primary production of organic matter as an indicator of the eutrophication in the northern Adriatic Sea, *Sci. Total Environ.*, *56*, 211–220.

Sommer, U. (1994), *Planktologie*, Springer, New York.

Thingstad, T. F., and F. Rassoulzadegan (1999), Conceptual models for the biogeochemical role of the photic zone microbial food web, with particular reference to the Mediterranean Sea, *Prog. Oceanogr.*, *44*, 271–286.

Vichi, M., M. Zavatarelli, and N. Pinardi (1998), Seasonal modulation of microbial mediated carbon fluxes in the northern Adriatic Sea: A model study, *Fish. Oceanogr.*, *7*, 182–190.

Vichi, M., P. Oddo, M. Zavatarelli, A. Colluccelli, G. Coppini, M. Celio, S. Fonda Umani, and N. Pinardi (2003), Calibration and validation of one dimensional complex marine biogeochemical fluxes model in different areas of the northern Adriatic shelf, *Ann. Geophys.*, *21*, 413–436.

Vichi, M., P. Ruardij, and J. W. Baretta (2004), Link or sink: A modelling interpretation of the open Baltic biogeochemistry, *Biogeosciences*, *1*, 79–100.

Vilicic, D., Z. Vucak, A. Skrivanic, and Z. Grzetic (1989), Phytoplankton blooms in the oligotrophic open south Adriatic waters, *Mar. Chem.*, *28*, 89–107.

Zavatarelli, M., and N. Pinardi (2003), The Adriatic Sea modelling system: A nested approach, *Ann. Geophys.*, *21*, 345–364.

Zavatarelli, M., F. Raicich, A. Artegiani, D. Bregant, and A. Russo (1998), Climatological biogeochemical characteristics of the Adriatic Sea, *J. Mar. Syst.*, *18*, 227–263.

Zavatarelli, M., J. W. Baretta, J. G. Baretta-Bekker, and N. Pinardi (2000), The dynamics of the Adriatic Sea ecosystem: An idealized model study, *Deep Sea Res., Part I*, *47*, 937–970.

Zavatarelli, M., N. Pinardi, V. H. Kourafalou, and A. Maggiore (2002), Diagnostic and prognostic model studies of the Adriatic Sea circulation: Seasonal variability, *J. Geophys. Res.*, *107*(C1), 3004, doi:10.1029/2000JC000210.

Zoppini, A., M. Pettine, C. Totti, A. Puddu, A. Artegiani, and R. Pagnotta (1995), Nutrients, standing crop and primary production in western coastal waters of the Adriatic Sea, *Estuarine Coastal Shelf Sci.*, *41*, 493–513.

S. Colella, Istituto di Scienze dell'Atmosfera e del Clima, CNR, Via Fosso del Cavaliere, 100, I-00133 Roma, Italy.

N. Pinardi, L. Polimene, and M. Zavatarelli, Università di Bologna, Centro interdipartimentale per la Ricerca sulle Scienze Ambientali, Via S. Alberto 163, I-48100 Ravenna, Italy. (l.polimene@sincem.unibo.it)